Supporting information

Graphene quantum dots wrapped gold nanoparticles with integrated enhancement mechanisms as sensitive and homogeneous substrates for Surface-Enhanced Raman Spectroscopy

Xuran Miao[†], Shengping Wen[†], Yu Su[†], Jiaju Fu[†], Xiaojun Luo[‡], Ping Wu[‡], Chenxin Cai[‡], Raz Jelinek[§], Li-Ping Jiang[*,†], and Jun-Jie Zhu[*,†]

† State Key Laboratory of Analytical Chemistry for Life Science, School of Chemistry and Chemical Engineering, Nanjing University, Nanjing 210023, China

‡ Nanjing Normal University, Jiangsu Key Laboratory of New Power Batteries, College of Chemistry & Materials Science, Nanjing 210097, China

§ Department of Chemistry, Ben Gurion University of the Negev, Beer Sheva 84105, Israel

*(L.-P.J) E-mail: jianglp@nju.edu.cn.

*(J.-J.Z) E-mail: jjzhu@nju.edu.cn.

Table of contents

- Additional experimental section
- Figure S1. Calculation of the enhancement factor for Au-NGQDs
- Figure S2. The HR-TEM and SAED pattern of Au-NGQDs
- Figure S3. HR-TEM characterization of Au-NGQDs under different hydrothermal time
- Figure S4. Characterization of NGQDs
- Figure S5. The TEM characterization of Au nanostar and Ag NPs
- Figure S6. Raman reproducibility of Au-NGQDs
- Figure S7. Colloidal stability of the Au-NGQDs
- Figure S8. Raman spectra of other aromatic molecules on Au NPs and Au-NGQDs NPs
- Figure S9. Raman effect of Au-NGQDs synthesized at different hydrothermal time
- Figure S10. Selection of laser excitation
- Figure S11. The electric field distribution of the Au and Au-NGQD NPs
- Figure S12. Optimizing the probe molecule concentration of MN-Au-NGQDs
- Figure S13. Toxicity test of MN-Au-NGQDs
- Figure S14. SERS mapping background
- Figure S15. Specificity and selectivity of MN-Au-NGQDs
- Figure S16. Optimization of probe incubation time
- Figure S17. Reproducibility of MN-Au-NGQDs in cell mapping

Additional Experimental Section

Chemicals and Reagents. Cetyltrimethylammonium bromide (CTAB), tris(hydroxymethyl) aminomethane (Tris), trisodium citrate dihydrate, and hydrogen tetrachloroaurate (III) trihydrate ($HAuCl_4 \cdot 3H_2O$) were purchased from Shanghai Chemical Reagent Co., Ltd. (Shanghai, China). Phosphate buffered saline (PBS) was ordered from Sangon Biotech Co., Ltd. (Shanghai, China). Cell toxicity assay kits were bought from KeyGEN BioTECH Co., Ltd. (Nanjing, China). Report molecules like 4-cyanobenzenethiol (MBN), 4-nitrobenzenethiol (4-NBT), 5,5'-dithiobis-(2-nitrobenzoic acid) (DTNB), rhodamine B (RB), rhodamine 6G (R6G), crystal violet (CV), 4-mercaptobenzoic acid (MBA), 4-mercaptophenylboronic acid (MPBA), 4-aminothiophenol (4-APT) were bought from Sigma-Aldrich(USA). All chemicals were of analytical reagent grade and used as received. Deionized water (DI water, 18 MΩ/cm) from a Millipore Auto purifier system was used for all the experiments.

Apparatus. Transmission electron microscopy (TEM) images were carried out on a JEM-2100 (200 kV) transmission electron microscope. High-resolution TEM, HAADF-STEM, and STEM-EDS images were obtained on a JEM-2800 transmission electron microscope. Field-emission scanning electron microscopy (FE-SEM) images were collected using a JSM-7800F scanning electron microscope (Hitachi Co., Japan). X-ray diffraction (XRD) patterns were recorded on a Philip-X'Pert X-ray diffractometer with a Cu Kα X-ray source. Raman spectra were collected with a Renishaw inVia confocal Raman spectrometer (Renishaw, UK) configured with a 50× objective lens (NA = 0.75) and an excitation laser of 633 nm. For recording SERS spectra, the static scan mode was used at a center of 1200 cm^{-1} with 10 s 1-exposure time and 100% laser power.

Preparation of citrated-stabilized Au seeds. Au seeds with an average size of 13 nm were synthetized according to a modified sodium citrate reduction procedure.[1] Typically, 100 mL of 1.0 mM $HAuCl_4$ aqueous solution was refluxed in a four-neck round bottom flask under vigorous agitation, followed by rapidly adding 10 mL of 1wt.% sodium citrate solution. When the mixed solution showing a wine red in color, the reaction was terminated immediately. Finally, the obtained colloidal Au seeds solution was filtered with a 0.22 μm nitrocellulose membrane, and then stored at 4 °C before use.

Synthesis of NGQDs. The NGQDs were synthesized with the same hydrothermal process of Au-NGQDs without addition of Au NPs. 30 mL of 0.1 M CTAB solution were transferred to a 50-mL Teflon-lined autoclave and heated at 165 °C in an oven for 1 h. The as-synthesized NGQDs were then dialyzed to release the redundant CTAB and stored in 4 ℃ for further use.

FDTD simulation. For simulating the electric filed intensity and distribution of Au-NGQDs, three-dimensional FDTD simulations from Lumerical Solutions, Inc. (Vancouver, Canada) were performed. We constructed a model composed of an inner 40 nm-diameter Au core coated with 2 nm-diameter and 0.35 nm-thickness NGQDs nanosheets, which were the mean sizes of the as-synthesized nanostructures. The boundary conditions of the simulation domain perfectly matched the layer absorbing boundaries. A total-field/scattered field source served as the incident light in the simulation region. The calculation region was $0.2\times0.2\times0.2$ μm^3, in which the grid resolution was set to 2 nm. Optical constants of the dielectric permittivity for gold as a function of the wavelength were adapted from the Johnson and Christy database included in the FDTD simulation. The refractive index of graphene in the visible range is governed by $n_g=3.0+C(\lambda_0/3)i$, which the constant $C\approx5.446$ μm^{-1} is obtained from the opacity measurement of previous report,[2] and λ_0 is the vacuum wavelength. The refractive index of the surrounding medium was set to be

1.33 for water.

DFT calculation. The charge distribution and band gap of Au, NGQDs and Au–NGQDs were theoretically calculated in the VASP codes,[3] based on density functional theory (DFT)[4] within the projector augmented wave (PAW).[5] The generalized gradient approximation (GGA) methods in the scheme of Perdew-Burke-Ernzerhof (PBE)[6] to describe the exchange and correlation potential. The electron wave functions were expanded in plane wave with an energy cutoff of 300 eV. The convergence criterion of optimal geometry which were based on the energy and force convergence are 1×10^{-4} and 2×10^{-2} eV/Å, respectively. Considering the calculated accuracy and efficiency, we modelled the 21×21 $Å^2$ unit cell of Au (111) plane as the platform for the adsorption of CV molecules. The lattice constants of supercell (containing vacuum layer in vertical direction) are larger than 20 Å, which is large enough to eliminate the interaction between the layer and its images.

SERS detection method. Typically, the flat PDMS film (thickness, 1 mm) composed of many open cavities (diameter/height, 5 mm/1 mm) was first prepared, and tightly pasted onto a clean glass slide to construct sample cells. After that, the solution with a fixed volume was added to the as-prepared PDMS cell, and then placed under a 633 nm Raman laser for further detection. Before signal collection, the laser beam focused on the glass surface at the bottom of PDMS cell, whose Z-axis position was set as the reference. Thereafter, Raman signals of the solution were collected after rising a 500 μm of Z-axis height. All the tests were conducted without changing Z-axis height to eliminate the detection depth effects.

Cell culture. MCF-7, HeLa, and L02 cells were cultured in Dulbecco's modified Eagle's medium (DMEM, GIBCO) supplemented with 10% of fetal calf serum, 100 μg mL^{-1} penicillin and 100 μg mL^{-1} streptomycin at 37 ºC in a humidified atmosphere with 5% CO_2, respectively. In

the logarithmic growth phase, these cells were harvested by trypsinogen, and thereafter resuspended in DMEM. Cell number was counted on a hemocytometer before all experiments.

SERS imaging of sialic acids (SAs) on MCF-7, HeLa, and L02 cell surfaces. MCF-7, HeLa, and L02 cells were separately seeded on confocal dishes and incubated at 37 °C for 24 h. Then the cell samples were subjected to incubate with 200 μL of MPBA/4-NBT@Au-NGQDs (1.0 nM MN-Au-NGQDs) for 60 min each. After each incubation step, the cells were washed twice with PBS to remove excess probe. Then the cells were fixed with paraformaldehyde solution for 15 min before Raman imaging. The Raman images of cells were obtained by the map image acquisition mode using static scan type at a center wavenumber of 1200 cm^{-1} with 1-s exposure time, 1-time accumulation, and 100% laser power.[7] The imaging step was 1 μm ×1 μm. The strongest characteristic peak of 4-NBT was at 1333 cm^{-1}, so the Raman images of cells were generated using signal to baseline map review mode from 1300 cm^{-1} to 1360 cm^{-1} by a WiRE 3.4 software, and the color scale of images were chosen as black to red, which corresponded to the background noise intensity and maximum signal intensity, respectively.

Cytotoxicity assay. The cytotoxicity experiments were carried out using a MTT assay kit.[8] In brief, 150 μL of MCF-7 cells suspension (6×10^4 cells per well) were respectively incubated with different concentrations of MN-Au-NGQDs probes in a 96-well plate for 1 h. After the incubation, MCF-7 cells were continuously cultured with 150 μL of DMEM containing MTT (0.5 mg L^{-1}) at 37 °C for another 4 h. Then, MCF-7 cells were washed via PBS, and dissolved in 100 μL DMSO. The absorbance of the resulting solution was measured on a Varioskan Flash multifunctional microplate reader (Thermo Fisher Scientific, USA) at the excitation of 570 nm. All experiments were repeated at least five times. The absorbance reflects the cell viability of

MCF-7 cells.

Calculation of SERS enhancement factor. Figure S1b illustrates the relationship between 4-NBT molecule concentration and SERS intensity, and a concentration of 4-NBT solution lower than 1.0 μM was used to prevent the supersaturated adsorption of probe molecule on Au-NGQDs generating false EF value. EF was calculated using the following equation (*Eq*. 1):[9]

$$\mathrm{EF} = \frac{I_{SERS}}{N_{SERS}} \Big/ \frac{I_{\mathrm{Bulk}}}{N_{\mathrm{Bulk}}} \qquad (1)$$

where I_{SERS} and I_{Bulk} are the intensities of the Raman peak at 1333 cm^{-1} for the individual Au-NGQDs NPs and the pure 4-NBT solution (0.1 nM, 10 mM), respectively; and N_{SERS} and N_{BULK} are the number of 4-NBT molecules on a single Au-NGQDs nanoparticle and within solution, respectively. The number of 4-NBT molecules on a single Au-NGQDs (N_{SERS}) was estimated by assuming that the maximum number of 4-NBT molecules were packed on the Au-NGQDs (average diameter of 40 nm). To estimate I_{Bulk} and N_{Bulk}, 10 μL of a 4-NBT solution (10 mM) was introduced into a sticker chamber placed on a glass substrate and illuminated with a 633 nm laser for 10 s through an objective lens (50×, NA = 0.5). Assuming that the effective excitation volume (V_{Bulk}) was a cylinder, the height (h) was calculated using the *Eq.* 2:[10]

$$\frac{h}{2r} = \frac{3.28\eta}{NA} \qquad (2)$$

where η is the refractive index of the medium (water; 1.33) and r is the radius of the laser beam (1 μm). Further, N_{Bulk} was calculated using the *Eq.* 3: [10]

$$N_{BULK} = \left(V_{\mathrm{Bulk}} \times \frac{D}{M}\right) \times N_A \qquad (3)$$

where D is the density of 4-NBT, M is the molar mass of 4-NBT, and NA is Avogadro's constant. As shown in Figure S1B, I_{SERS} and I_{Bulk} were found to be 115786.3 and 1052 counts, respectively. Therefore, the EF was calculated to be 2.01×10^{6}.

Additional Results

1. Calculation of the enhancement factor for Au-NGQDs

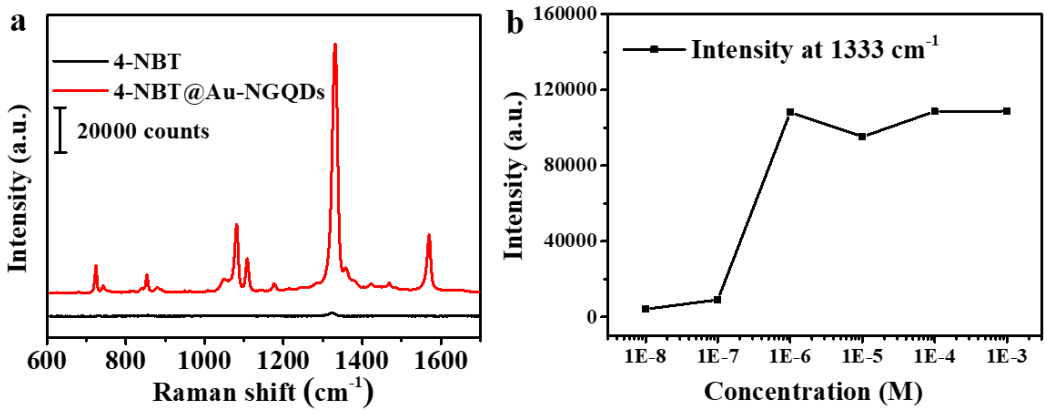

Figure S1. (a) Representative Raman spectra of 4-NBT solution (10 mM) and 4-NBT@Au-NGQDs NP (0.1 nM). (b) The relationship between the peak intensity at 1333 cm^{-1} and various concentrations of 4-NBT adsorbed on single Au-NGQDs NP. The average SERS spectrum was calculated from 10 times independent replicates.

2. The HR-TEM and SAED pattern of Au-NGQDs

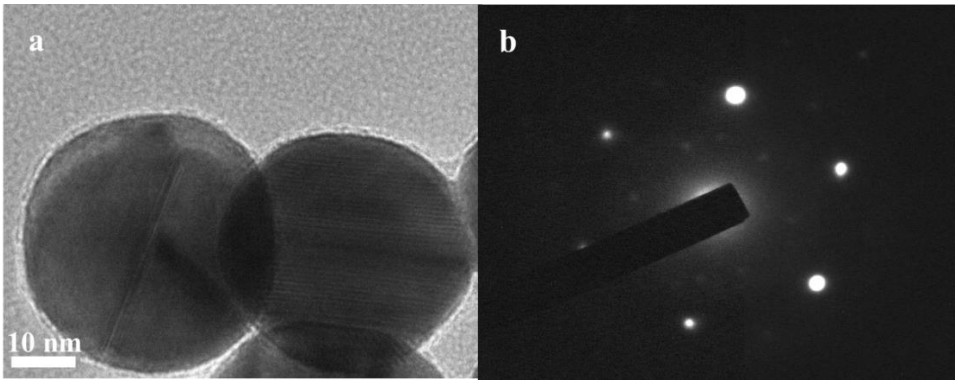

Figure S2. (a) The HR-TEM and (b) SAED pattern of Au-NGQDs.

3. HR-TEM characterization of Au-NGQDs under different hydrothermal time

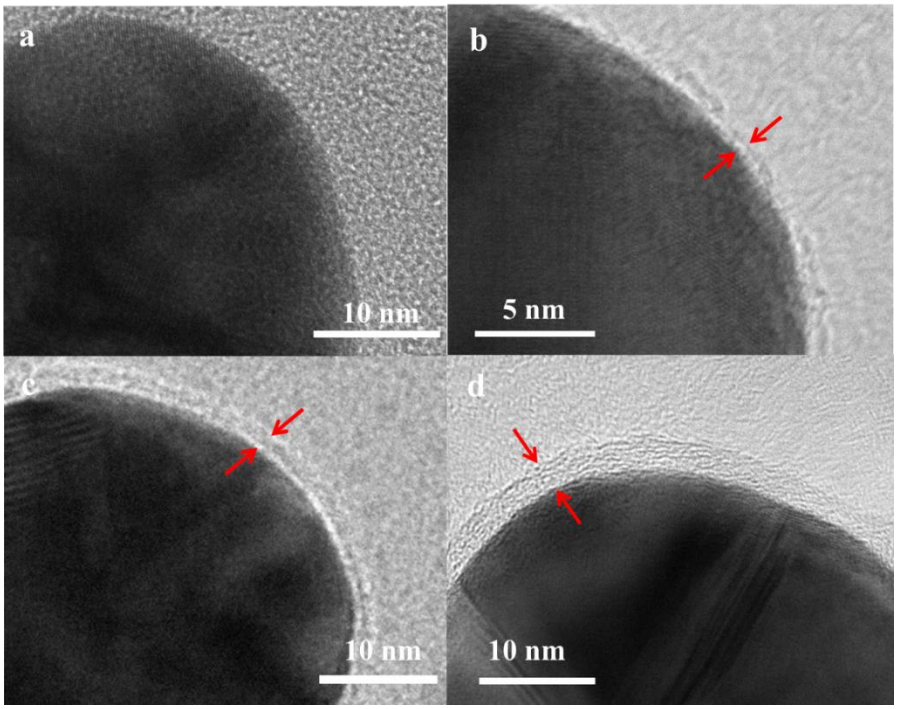

Figure S3. HR-TEM images of Au-NGQDs NPs and morphology of NGQDs of different hydrothermal time. (a) 0.5 h; (b) 1 h; (c) 2 h; (d) 3 h.

4. Characterization of NGQDs

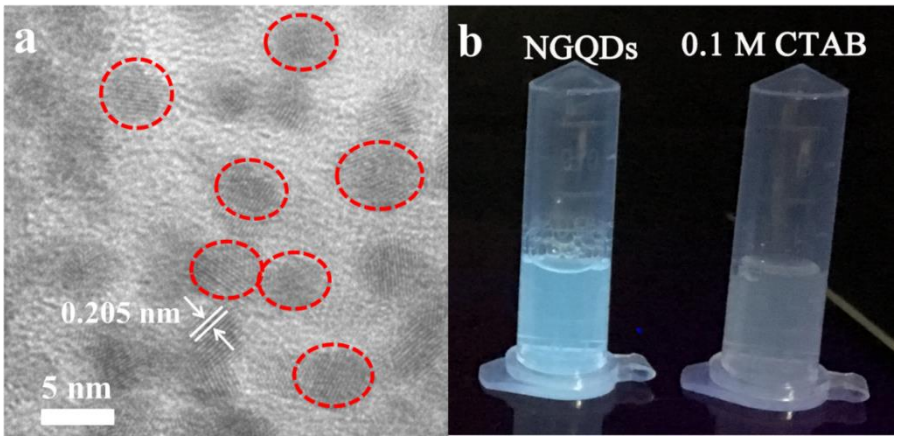

Figure S4. (a) The HR-TEM image of NGQDs synthesized by 0.1 M CTAB. (b) Photographs of NGQDs (left), and 0.1 M CTAB solution (right) under UV light irradiation.

5. The TEM characterization of Au nanostar and Ag NPs

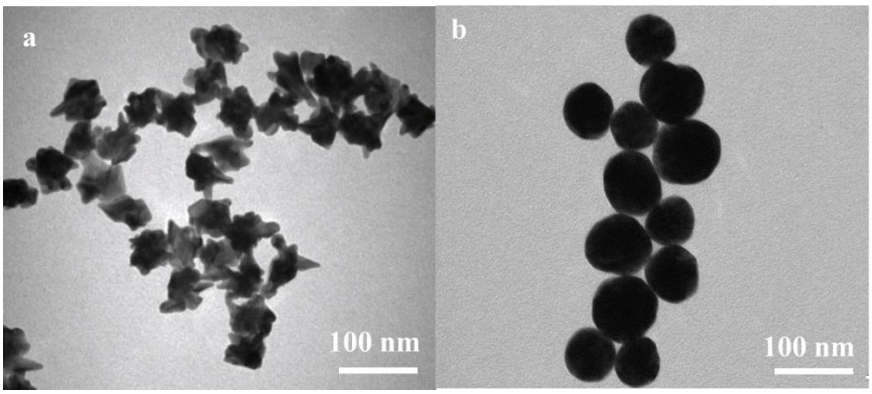

Figure S5. The TEM image of (a) Au nanostar; (b) Ag NPs

6. Raman reproducibility of Au-NGQDs

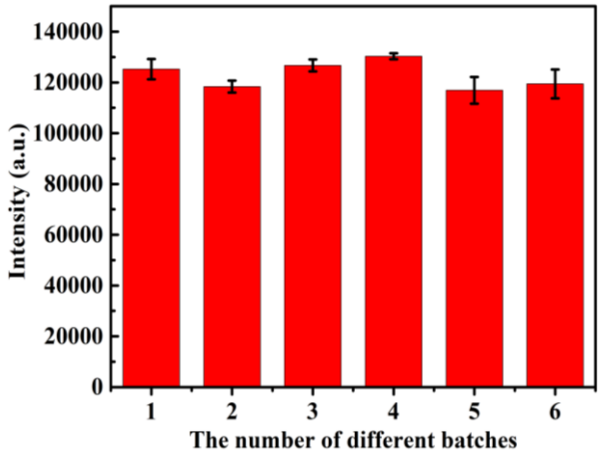

Figure S6. Raman signal intensity at 1333 cm^{-1} of 4-NBT on different batches of Au-NGQDs. The results show that a relative standard deviation (RSD) of 4.4% was obtained for Raman intensities at 1333 cm^{-1}, indicating high signal reproducibility between different batches of Au-NGQDs. Error bars represent the standard deviations of signal intensity collected from 15 random spots on the same sample.

7. Colloidal stability of the Au-NGQDs

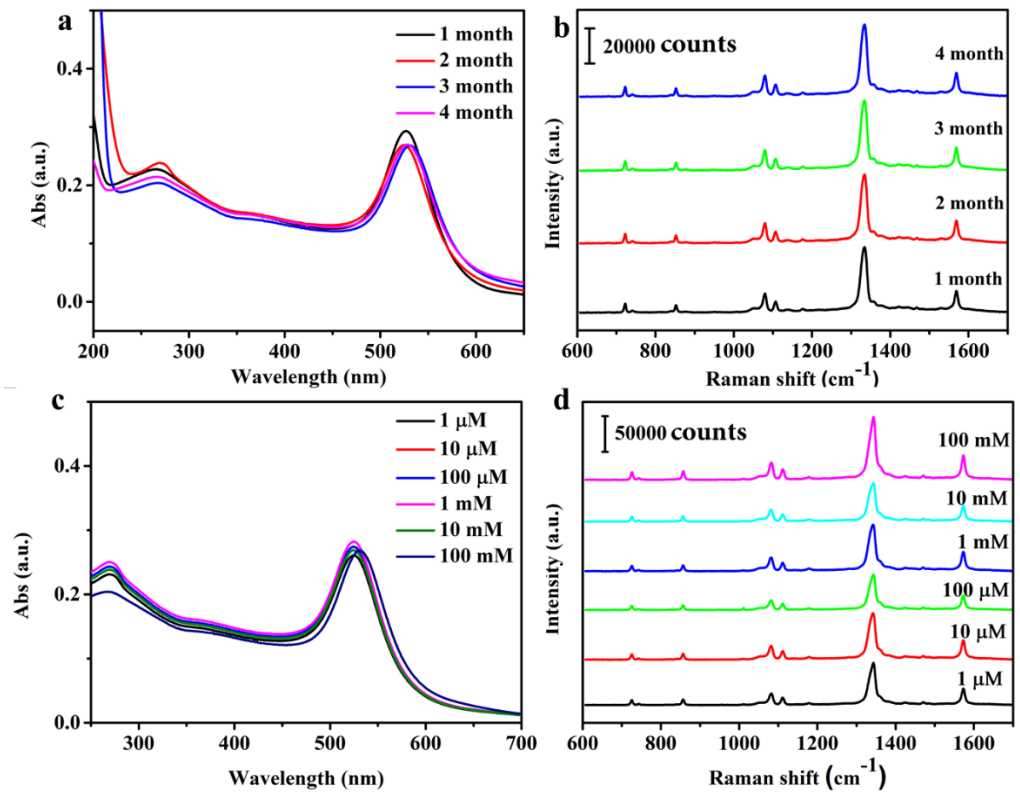

Figure S7. Investigating the colloidal stability of the Au-NGQDs during the long time storage and NaCl existing by measuring (A) UV-vis spectra and (B) SERS spectra of 4-NBT on the nanoparticles in the periods of 1 to 4 month, the results show that a relative standard deviation of 4.0% was obtained for Raman intensities at 1333 cm^{-1}. (C) UV-vis spectra of Au-NGQDs in different concentrations of NaCl solutions. (D) Comparing the SERS spectra of 4-NBT obtained from Au-NGQDs dispersed in different concentrations of NaCl solutions, the RSD of obtained Raman intensities at 1333 cm^{-1} is 5.6%.

8. Raman spectra of other aromatic molecules on Au NPs and Au-NGQDs NPs

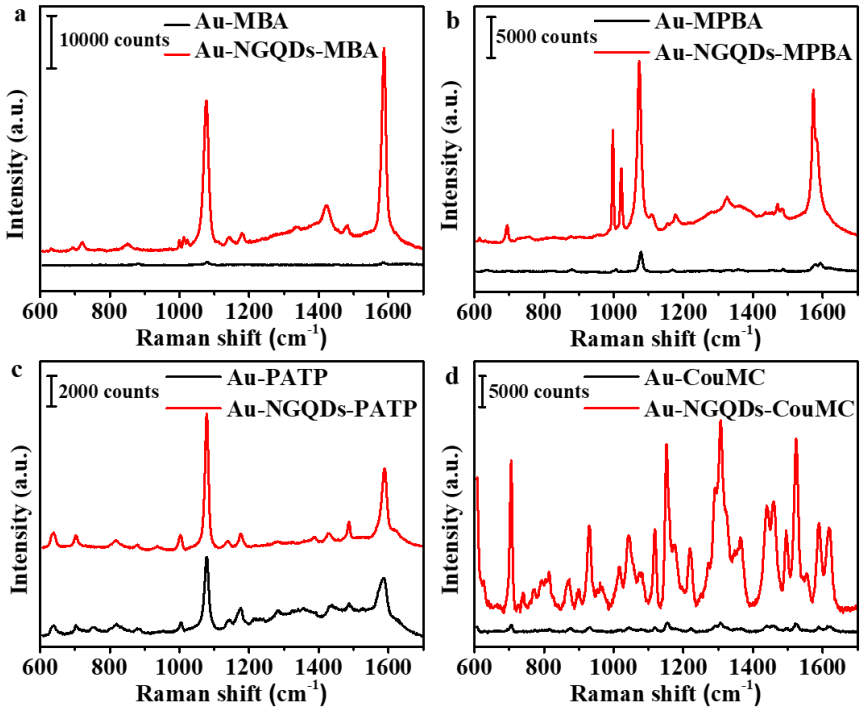

Figure S8. Raman spectra of (a) MBA; (b) MPBA; (c) PATP; (d) CouMC on Au NPs (black line) and Au-NGQDs NPs (red line).

9. Raman effect of Au-NGQDs synthesized at different hydrothermal time

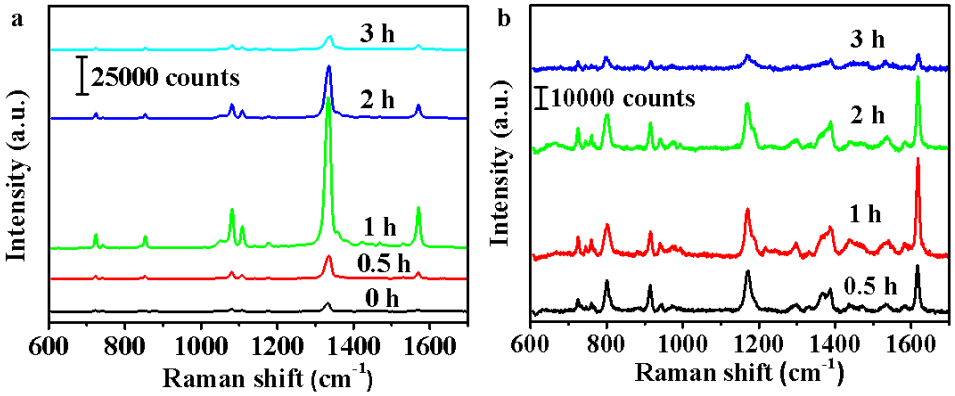

Figure S9. Raman spectra of Au-NGQDs synthesized at different hydrothermal time at 0, 0.5, 1, 2, and 3 h when V_{AuNPs}/V_{CTAB} is 2:1. (a) 4-NBT; (b) CV.

10. Selection of laser excitation

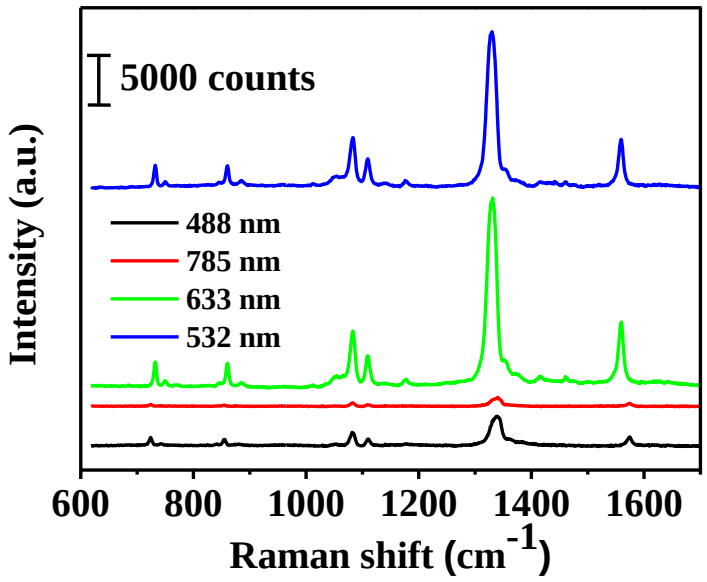

Figure S10. The SERS spectrum of 4-NBT@Au-NGQDs NP (0.1 nM) under different laser excitation.

11. The electric field distribution of the Au and Au-NGQDs

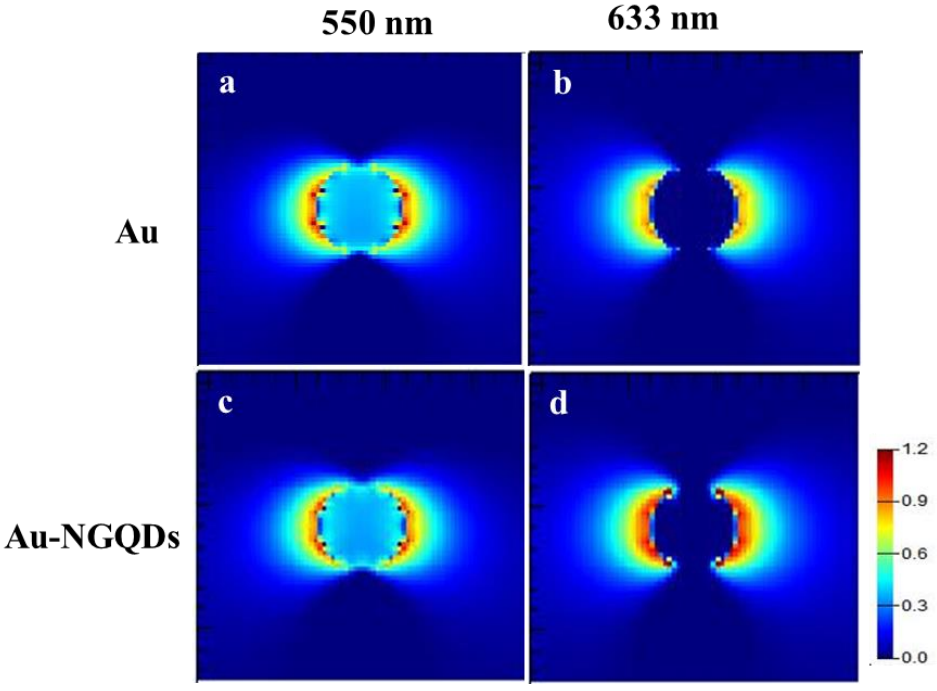

Figure S11. The electric field distribution of the Au (top line) and Au-NGQD NPs (bottom line) obtained at the wavelength of 550 nm (left line) and 633 nm (right line) respectively.

12. Optimizing the probe molecule concentration of MN-Au-NGQDs

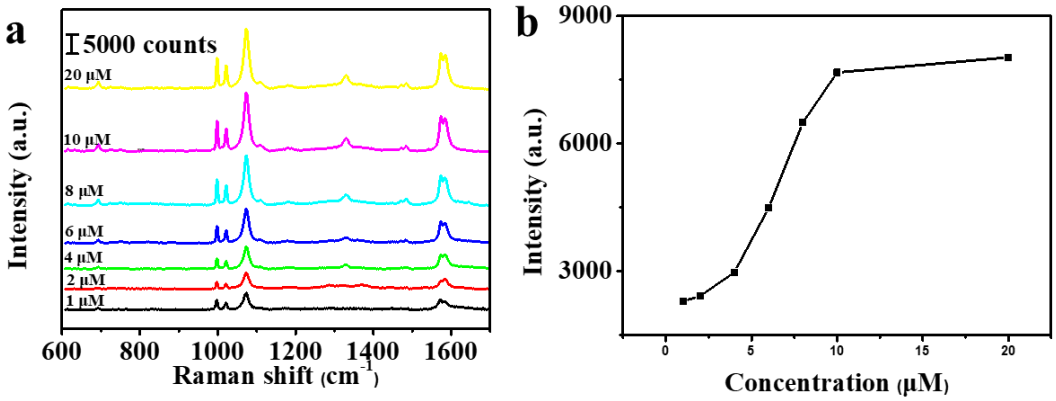

Figure S12. (a) The SERS spectrum of MPBA@Au-NGQDs NPs with the different concentration of MPBA. (b) The relationship between the peak intensity at 1333 cm^{-1} and various concentrations of MPBA adsorbed on Au-NGQDs NPs. The measured SERS spectrum was obtained by taking the average of thrice measurements.

13. Toxicity test of MN-Au-NGQDs

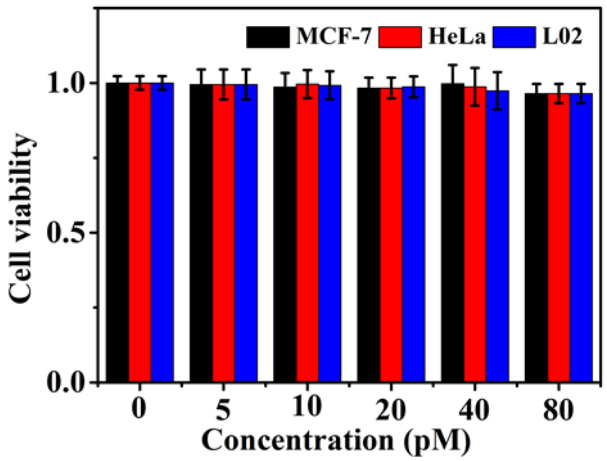

Figure S13. Cell viability of MCF-7, HeLa, and L02 cells incubated with the different concentration of Au-NGQDs probes for 1 h. Error bars represent the standard deviations of cell viability calculated from five sample replicates.

14. SERS mapping background

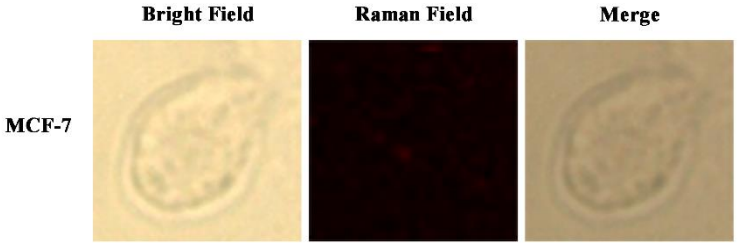

Figure S14. SERS images of MCF-7 cell without using any SERS probe (left: bright field; middle: SERS mapping images based on the intensity of 1333 cm^{-1}; right: merged images)

15. Specificity and selectivity of MN-Au-NGQDs

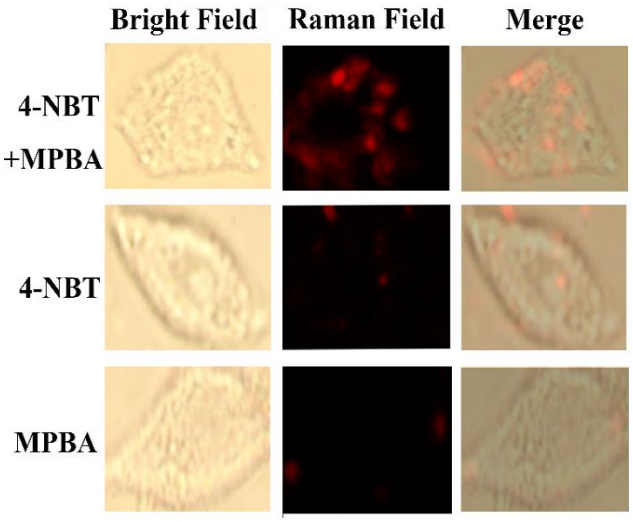

Figure S15. SERS images of MCF-7 cell using MPBA@Au-NGQDs, 4-NBT@Au-NGQDs and MPBA/4-NBT@Au-NGQDs NPs probes (left: bright field; middle: SERS mapping images based on the intensity of 1333 cm^{-1}; right: merged images)

16. Optimization of probe incubation time

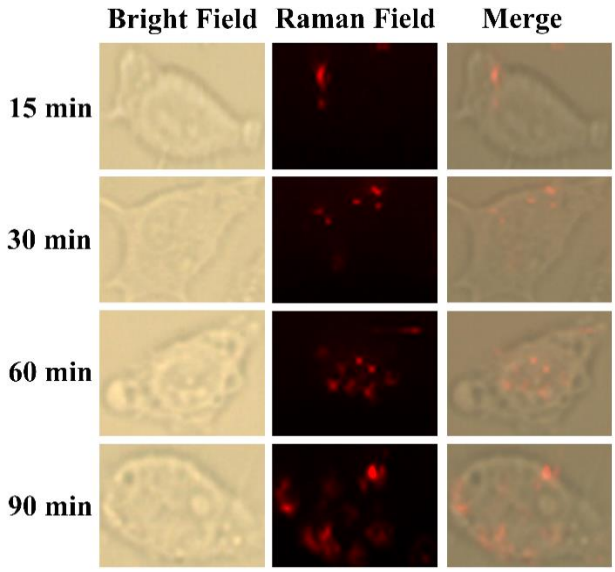

Figure S16. SERS images of MCF-7 cell under different probe incubation time (left: bright field; middle: SERS mapping images based on the intensity of 1333 cm^{-1}; right: merged images)

17. Reproducibility of MN-Au-NGQDs in cell mapping

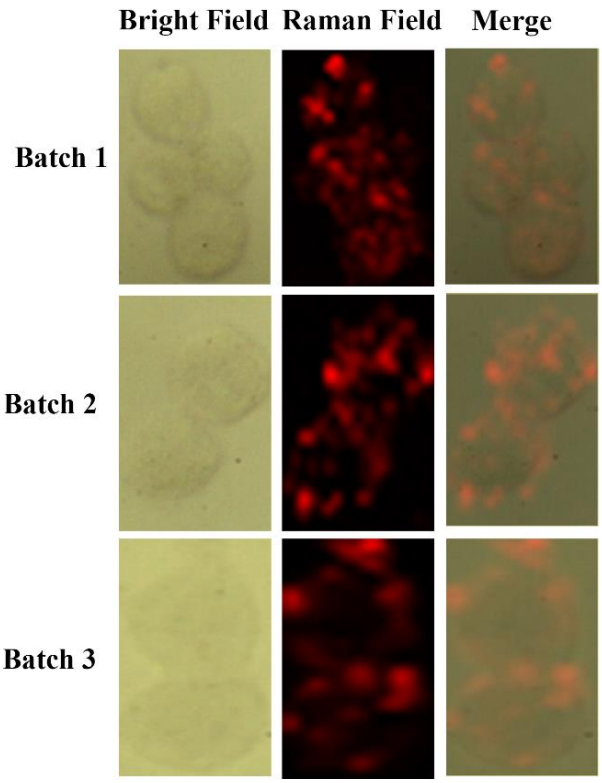

Figure S17. SERS images of MCF-7 cell with different batches (left: bright field; middle: SERS mapping images based on the intensity of 1333 cm^{-1}; right: merged images).

References

(1) Ziegler, C.; Eychmüller, A. seended growth synthesis of uniform gold anoparticles with diameters of 15−300 nm, *J. Phys. Chem. C* **2011**, *115*, 4502-4506.

(2) Ouyang, L.; Hu, Y.; Zhu, L.; Cheng, G. J.; Irudayaraj, J. A reusable laser wrapped graphene-Ag array based SERS sensor for trace detection of genomic DNA methylation, *Biosens. Bioelectron.* **2017**, *92*, 755-762.

(3) G. Kresse, J. F. l. Efficient iterative schemes for ab initio total-energy calculations using a plane-wave basis set, *Phys. Rev. B* **1996**, *54*, 11169-11186.

(4) Hohenberg, P.; Kohn, W. Inhomogeneous electron gas, *Phys. Rev*. **1964**, *136*, B864-B871.

(5) Blöchl, P. E. Projector augmented-wave method, *Phys. Rev. B* **1994**, *50*, 17953-17979.

(6) John P. Perdew, K. B., Matthias Ernzerhof. Generalized gradient approximation made simple, *Phys. Rev. Lett*. **1996**, *77*, 3865-3868.

(7) Song, W.; Ding, L.; Chen, Y.; Ju, H. Plasmonic coupling of dual gold nanoprobes for SERS imaging of sialic acids on living cells, *Chem. Commun.* **2016**, *52*, 10640-10643.

(8) Wen, S.; Su, Y.; Wu, R.; Zhou, S.; Min, Q.; Fan, G. C.; Jiang, L. P.; Song, R. B.; Zhu, J. J. Plasmonic Au nanostar Raman probes coupling with highly ordered TiO_2/Au nanotube arrays as the reliable SERS sensing platform for chronic myeloid leukemia drug evaluation, *Biosens Bioelectron* **2018**, *117*, 260-266.

(9) Wang, X.; Shi, W.; Jin, Z.; Huang, W.; Lin, J.; Ma, G.; Li, S.; Guo, L. Remarkable SERS activity observed from amorphous ZnO nanocages, *Angew. Chem.Int. Edit*. **2017**, *56*, 9851-9855.

(10) Kim, M.; Ko, S. M.; Kim, J. M.; Son, J.; Lee, C.; Rhim, W. K.; Nam, J. M. Dealloyed intra-nanogap particles with highly robust, quantifiable surface-enhanced Raman scattering signals for biosensing and bioimaging applications, *ACS Central Sci*. **2018**, *4*, 277-287.